

Continuous Approximation of the Fully Connected Ising Hamiltonian: Exact Ground State Solutions for a Novel Class of Ising Models with Applications to Fidelity Assessment in Ising Machines

Amirhossein Rezaei^{1,*}, Mahmood Hasani^{2,†}, Alireza Rezaei^{2,‡} and Seyyed M. Hassan Halataei^{1,§}

¹ Department of Physics, Shahid Beheshti University, G.C. Evin, Tehran 19839, Iran and

² Department of Electrical Engineering, Amirkabir University of Technology, Iran

(Dated: December 2, 2024)

In this study, we present a novel analytical approach to solving large-scale Ising problems by reformulating the discrete Ising Hamiltonian into a continuous framework. This transformation enables us to derive exact solutions for a non-trivial class of fully connected Ising models. To validate our method, we conducted numerical experiments comparing our analytical solutions with those obtained from a quantum-inspired Ising algorithm and a quantum Ising machine. The results demonstrate that the quantum-inspired algorithm and brute-force method successfully align with our solutions, while the quantum Ising machine exhibits notable deviations. Our method offers promising avenues for analytically solving diverse Ising problem instances, while the class of Ising problems addressed here provides a robust framework for assessing the fidelity of Ising machines.

I. INTRODUCTION

The Ising model [1, 2], originated from statistical mechanics, is a mathematical model used to study and describe spin glasses. This model consists of a binary spin system with energy defined by the Ising Hamiltonian [3]. A key problem of interest is determining the ground state energy of the Ising model. Specifically, the *Ising problem* involves finding the configuration of N Ising spins, $s_i = \pm 1$, that minimizes the Hamiltonian:

$$H = \sum_{1 \leq i < j \leq N} J_{ij} s_i s_j, \quad (1)$$

where a real number J_{ij} denotes a coupling constant between every two of the N Ising spins. As each s_i can adopt one of the two states, the configuration space for N spins comprises 2^N possibilities. Consequently, determining the ground state energy of Ising model is generally an NP-hard problem. That is, every problem in the complexity class of NP, can be reduced (mapped) to the Ising model [4]. The Ising model has been the subject of studying NP-complete problems as well [5]. This includes several classical problems such as the Max-Cut [6], the Travelling Salesman Problem [7], Set Cover [6], Knapsack with Integer Weights [8], Graph Coloring [9] and Clique Cover [10].

Identifying and validating the exact ground state of the Ising Hamiltonian generally remains an unsolved problem. To find the ground state energy and configuration, Ising minimizers such as D-Wave quantum annealer [11–13], Coherent Ising Machine [14–17], Bifurcation-based adiabatic quantum computation [18–20] and Simulated Annealing [21–23] are used. However, a few specific analytical solutions also exist in literature. [24] provides an exact prob-

able solution for a periodic lattice by transforming the problem into MAX-SAT and MAX-MIN optimization problems. [25] found the ground state for Shastry-Sutherland lattice in presence of a magnetic field. Both of these solutions assume a finite interaction range, i.e. non-fully connected. Also, these solutions are only valid for uniform interaction couplings (where all elements have a fixed, equal value). Some notable work that go beyond these limitations are: [26], which demonstrated that the Ising model with long-range antiferromagnetic interactions exhibits a complete devil's staircase. [27] also studied a system with competing short-range ferromagnetic coupling and long-range antiferromagnetic Coulomb interactions. In their study, they observed specific periodic configurations as the ground state.

In this paper, we introduce a class of fully connected Ising models. We reformulate the Ising Hamiltonian as a continuous function, enabling a novel analytical approach to solving the model and determining its ground state. To assess the effectiveness of this method, we conduct numerical experiments for validating our analytical solution, involving brute-force calculations, the Simulated Coherent Ising Machine [28–31] (SimCIM) and the D-Wave quantum computer. This class of Ising Hamiltonian could serve as a framework for assessing the fidelity of Ising minimizers. The results demonstrate perfect agreement between brute-force calculations and our analytical approach, as well as between SimCIM and our method. However, the D-Wave quantum solver exhibits significant deviations for larger problem sizes.

To enhance the readability of the paper, we first present our Ising model, followed by our method for solving it, and conclude with benchmarks and comparisons.

II. THE INTERACTION MATRIX

First, we introduce the interaction matrix:

$$J_{ij}^{(N,d)} = \frac{1}{Nd} (i^d + j^d) (1 - \delta_{ij}), \quad (2)$$

* rezaeamirhosein@gmail.com

† mahmoodhasaniph@gmail.com

‡ alirezarezaei8080@gmail.com

§ m_halataei@sbu.ac.ir

where i and j are the indices of the matrix $J^{(N,d)}$, with d being a real value. The variable N is the size of the matrix. The terms i^d and j^d denote the indices i and j raised to the power of d , respectively. As an example, for the size of $N = 5$ and $d = 2$ we have:

$$J^{(5,2)} = \frac{1}{5^2} \begin{bmatrix} 0 & 5 & 10 & 17 & 26 \\ 5 & 0 & 13 & 20 & 29 \\ 10 & 13 & 0 & 25 & 34 \\ 17 & 20 & 25 & 0 & 41 \\ 26 & 29 & 34 & 41 & 0 \end{bmatrix}. \quad (3)$$

The ground state configuration for this class of interaction matrices is postulated to follow the pattern shown in Equation (4). The proof substantiating this postulation will be provided in the subsequent section.

$$\mathbf{s}_g = \begin{bmatrix} 1 \\ 1 \\ \vdots \\ 1 \\ -1 \\ -1 \\ \vdots \\ -1 \end{bmatrix}. \quad (4)$$

In this configuration, the up spins are adjacent to each other, as are the down spins. We denote the number of up spins by M , and the number of down spins by $N - M$. This means we can represent the ground state with only one variable, M . As an example, for the $J^{(5,2)}$ the ground state is: $\mathbf{s}_g^{(5,2)} = [1, 1, 1, -1, -1]$, which has 3 up spins and 2 down spins. The Ising Hamiltonian (Equation (1)) is invariant under gauge transformation, i.e. all of the eigenstates of Equation (1) are doubly-degenerate. In our notation, we consider the first cluster size as the up spin (M).

III. GROUND STATE PATTERN

As $J^{(N,d)}$ is symmetric, the following is true:

$$H = \sum_{1 \leq i < j \leq N} J_{ij}^{(N,d)} s_i s_j = \frac{1}{2} \sum_{i=1}^N \sum_{j=1}^N J_{ij}^{(N,d)} s_i s_j. \quad (5)$$

Since the ground state configuration consists of M adjacent up spins and $N - M$ adjacent down spins, the \mathbf{ss}^T matrix can be visualized as depicted in Figure 1.

In this visualization, the upper left and lower right quadrants represent interactions between spins with the same orientation, i.e. $s_i s_j = 1$. Furthermore, the other two quadrants represent interactions between spins with different orientations, i.e. $s_i s_j = -1$. Note that this diagram depicts the sign of the interactions between spins, not the coupling values themselves.

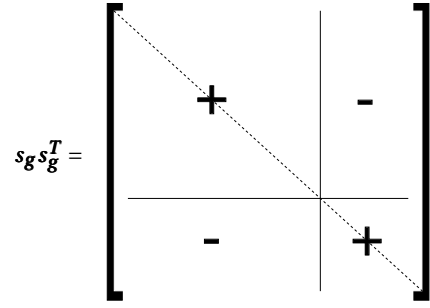


FIG. 1. Sign of interactions between spins, denoted by \mathbf{ss}^T and represented as a matrix.

If we assume the ground state is represented by Equation (4), we can proceed as follows. By considering the upper left quadrant as an $M \times M$ matrix, we can rewrite the Hamiltonian (Equation (5)) in the following form:

$$H(M, N, d) = \frac{1}{2N^d} \left\{ \sum_{1 \leq i \neq j \leq M} (i^d + j^d) + \sum_{M+1 \leq i \neq j \leq N} (i^d + j^d) - \sum_{i=1}^M \sum_{j=M+1}^N (i^d + j^d) - \sum_{i=M+1}^N \sum_{j=1}^M (i^d + j^d) \right\}, \quad (6)$$

where the first and second term correspond to interactions between spins which have the same orientation, i.e. $s_i s_j = 1$. The third and fourth term, correspond to the interactions between spins with opposite orientation, such that: $s_i s_j = -1$.

Considering the following formula [32]:

$$F^d(N) = \sum_{i=1}^N i^d = \sum_{r=0}^d \frac{(-1)^r B_r}{d+1} \binom{d+1}{r} N^{d+1-r}, \quad (7)$$

where B_r is the r th Bernoulli number. We can write Equation (6), in terms of Equation (7) as follows:

$$H(M, N, d) = \frac{1}{N^d} \left((N - 4M + 1) F^d(N) - 4(N - 2M) F^d(M) \right) \quad (8)$$

Now to find the ground state energy and configuration, we just need to find the M that minimizes H :

$$M_g^{(N,d)} = \underset{M}{\operatorname{argmin}} H(M, N, d), \quad (9)$$

Given that M is an integer within the range $[1, N]$, the complexity of the problem becomes $\mathcal{O}(N)$, which is obviously polynomial.

As N grows, the ratio $\frac{M}{N}$ stabilizes to a constant. We denote this constant ratio as q . As q varies by unit of $\frac{1}{N}$, in the limit of large N this change becomes very small, thus we can treat q as a continuous variable. Our next step is to determine the value of q in the large N limit. To do so, we minimize the function H with respect to q :

$$\frac{\partial H(M, N, d)}{\partial q} = 0. \quad (10)$$

In Equation (8), by considering terms which are dependent on M and discarding $\frac{4}{N^d}$, we only need to minimize the Equation (11) as written below:

$$\tilde{H}(M, N, d) = MF^d(N) + (N - 2M)F^d(M). \quad (11)$$

Using $M = qN$, Equations (10) and (11) we arrive at:

$$N\{F^d(N) - 2F^d(M) + (1 - 2q)\frac{\partial F^d(M)}{\partial M}\frac{\partial M}{\partial q}\} = 0. \quad (12)$$

Derivative of Equation (7) is:

$$\frac{\partial F^d(M)}{\partial M} = dF^{d-1}(M) + (-1)^d B_d. \quad (13)$$

Substituting Equation (13) in Equation (12) we get:

$$F^d(N) - 2F^d(M) + (1 - 2q)N\{F^{d-1}(M) + (-1)^d B_d\} = 0. \quad (14)$$

Keeping the the first leading order term in Equation (7) results in:

$$F^d(N) \approx \frac{N^{d+1}}{d+1} B_0, \quad (15)$$

and substituting it in Equation (14), we can write as below:

$$\frac{B_0 N^{d+1}}{d+1} (1 - 2q^{d+1}) + (1 - 2q)N((qN)^d B_0 + (-1)^d B_d) = 0. \quad (16)$$

If we multiply both sides by $\frac{d+1}{B_0 N^{d+1}}$, for large N , $\frac{B_d}{N^{d+1}}$ tends to zero and we arrive at the final Equation:

$$1 + (1 + d)q^d - 2(2 + d)q^{d+1} = 0. \quad (17)$$

For $d \notin \{1, 2, 3\}$, Equation (17) becomes a transcendental equation and does not have a closed form solution. In these cases, we resort to numerical methods (such as the Newton-Raphson method) to find the roots of the equation.

IV. THEORETICAL APPROACH TO FIND THE GROUND STATE PATTERN

Now note that *any* spin configuration could be represented as Equation (18), which consists of an arbitrary number of domains of up and down spins. Each domain can contain one or more spins of the same orientation:

$$\mathbf{s}^T = [\underbrace{1 \ 1 \ \dots \ 1}_{c_1} \ \underbrace{-1 \ -1 \ \dots \ -1}_{c_2} \ \dots \ \underbrace{1 \ 1 \ \dots \ 1}_{c_\Lambda} \ \underbrace{-1 \ -1 \ \dots \ -1}_{c_{\Lambda+1}}]. \quad (18)$$

In continuous limit, the following function is equivalent to Eq. (18):

$$S(x, \mathbf{q}) = (-1)^\Lambda \prod_{\alpha=1}^{\Lambda} \text{sgn}(x - q_\alpha) \quad (19)$$

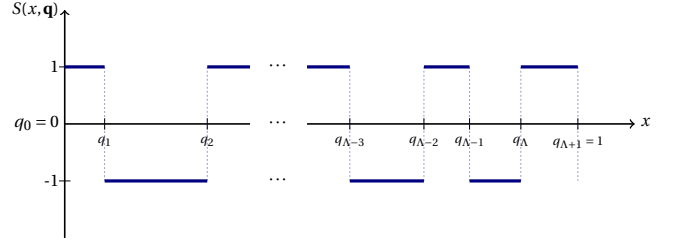


FIG. 2. Visualization of arbitrary spin configurations in continuous form. q_Λ denote the boundaries of each cluster, which consists of spins with the same orientation. In this figure $q_0 = 0$ and $q_{\Lambda+1} = 1$.

Figure 2, is a visualization of Equation (19). Each spin domain, denoted by c_i with $i \in [1, \Lambda + 1]$, occupies a certain region whose right boundary is denoted by q_α with $\alpha \in [1, \Lambda]$; the set of boundaries q_α can also be represented as a vector and for convenience, let's put $q_0 = 0$ and $q_{\Lambda+1} = 1$ which can be denoted by Equation (20)

$$\mathbf{q} = (q_1, q_2, \dots, q_\Lambda) \quad , \quad 0 < q_\alpha < 1 \quad , \quad q_{\alpha+1} > q_\alpha \quad (20)$$

Now, by neglecting the Kronecker delta in Equation (5) which just adds a constant term to the Hamiltonian, we can write as below:

$$H = \frac{1}{2} \sum_{i=1}^N \sum_{j=1}^N J_{ij}^{(N,d)} s_i s_j = \frac{N^2}{2} \sum_{i=1}^N \sum_{j=1}^N \left(\left(\frac{i}{N}\right)^d + \left(\frac{j}{N}\right)^d \right) s_i s_j \Delta i \Delta j. \quad (21)$$

where $\Delta i = \Delta j = \frac{1}{N}$. Summing Equation (21) over indices i and j is equivalent to a Riemann sum, which is defined as:

$$\sum_{i=1}^N f(x_i^*) \Delta x_i = \int_a^b f(x) dx \pm \mathcal{O}\left(\frac{(f(b) - f(a))(b - a)}{N}\right) \quad (22)$$

where $\Delta x_i = x_i - x_{i-1}$ and $x_i^* \in [x_{i-1}, x_i]$ and $x_0 = a < x_1 < x_2 < \dots < x_{N-1} < x_N = b$. Thus, it can be treated as an integral by setting $(\frac{i}{N})^d = x$ and $(\frac{j}{N})^d = y$ and $\Delta x = \frac{1}{N}$ and taking its limit for large N . We should note that for smooth function this method works appropriately but for not integrable functions the error term in Equation (22) diverges. By replacing s_i and s_j in Equation (21) with $S(x, \mathbf{q})$ and $S(y, \mathbf{q})$ respectively, which are defined in Equation(19) and using Equation (22) twice:

$$H_\Lambda(d, \mathbf{q}) = \frac{N^2}{2} \times \int_0^1 \int_0^1 \{(x^d + y^d) \prod_{\alpha=1}^{\Lambda} \text{sgn}(x - q_\alpha) \text{sgn}(y - q_\alpha)\} dx dy + \mathcal{O}(N) \quad (23)$$

where the term $\prod_{\alpha=1}^{\Lambda} \text{sgn}(x - q_\alpha) \text{sgn}(y - q_\alpha)$ is the continuous form of $\mathbf{s} \mathbf{s}^T$ and $y_i = \frac{i}{N}$. Moreover, using Equation (22) to obtain Equation (23) we have an error term which can be neglected in this problem due to large N , thus we can not use this method for any arbitrary Ising problem for finding the ground state pattern if the derivative of the integrand

does not exist. Note that this integral only has solution for $d > -1$. Evaluation of Equation (23) leads to Equation (24) where the details can be followed in Appendix B.

$$H_\Lambda(d, \mathbf{q}) = \frac{N^2}{1+d} \times \left((-1)^\Lambda + 2 \sum_{\alpha=1}^{\Lambda} (-1)^{\alpha+1} q_\alpha \right) \left((-1)^\Lambda + 2 \sum_{\alpha=1}^{\Lambda} (-1)^{\alpha+1} q_\alpha^{d+1} \right) \quad (24)$$

The minimum value of H_1 is always negative and exhibits convexity in the interval $q_1 \in (0, 0.5)$ for $d \in (-1, 0)$ and on the interval $q_1 \in (0.5, 1)$ for $d > 0$. In Appendix C we demonstrate that for $d > 0$, the term in parentheses on the left-hand side of Equation (C4) is strictly greater than 1, which leads to $\frac{1}{2} < q < 1$. This again implies that Eq. (C7) is always positive. Similar as before, we can show that for $d \in (-1, 0)$, $0 < q < \frac{1}{2}$ and the root is unique. This implies that the critical value for q_1 is unique. This can be shown using the mean value theorem which is discussed in more detail in Appendix C.

For $\Lambda \geq 2$, it can be shown that the minimum value of H_Λ is greater than the minimum value for H_1 thus proving that the minimum of H_Λ is obtained by setting $\Lambda = 1$, meaning the ground state pattern consist of two clusters only. More details can be found in Appendix D.

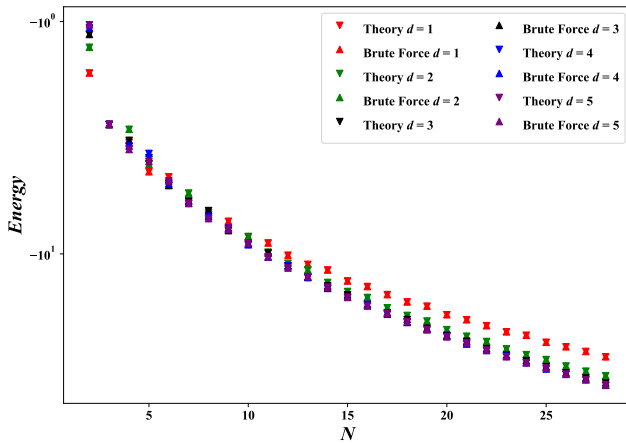


FIG. 3. The ground state energy, computed for $d \in [1, 5]$ and $N \in [1, 28]$, using brute force approach (up triangle) and by obtaining the value of M from Equation (9) and substituting in Equation (8) (down triangle)

V. NUMERICAL RESULTS

A. Simulated Coherent Ising Machine and Brute-Force Method

Now we calculate numerical results regarding the ground state of the system, described by equation (8). In Figure 3, we employed theoretical calculations for $d = 1, 2, 3, 4, 5$. To

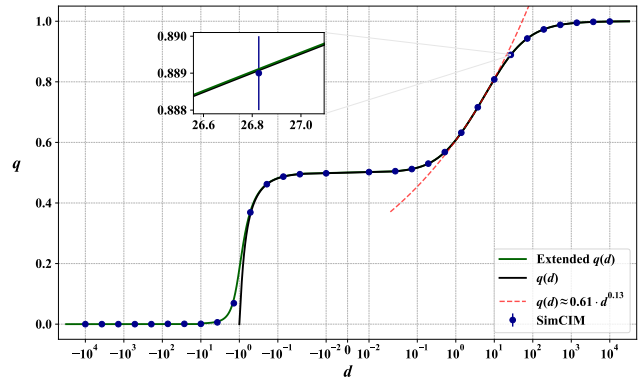


FIG. 4. In the ground state configuration, the up spins are adjacent to each other, as are the down spins. We denote the number of up spins as M . This means we can represent the ground state with only one variable, M . For large N , the ratio q stabilizes to a constant. This figure, depicts the plot of q against d (-10^4 to 10^4). Dark line: root of equation (17). Green line: root of equation (D6). Blue dots: SimCIM results. Error bars denote $\frac{1}{N}$ precision ($N = 1000$). Power law is observed for $d \in [1, 10]$, followed by saturation towards 1. At $d = 10$, $q \approx 0.81$.

validate our results, we also conducted brute force search to determine the ground state of the system described by equation (8) for each d value, across Ising problem sizes ranging from 2 to 28. Figure 3 shows that the energy values of our calculations and brute force search are exactly aligned. For larger systems, determining the ground state via brute force becomes infeasible due to the exponential increase in computational resources required.

For larger Ising problem sizes, particularly for $N = 1000$ as depicted in Figure 4, we exploited a Simulated Coherent Ising Machine. The results from this simulation, which completely agree with Equation (17), were obtained using the Chaotic Amplitude Control (CAC) algorithm. Details of the hyperparameter tuning of CAC is presented in the Appendix A.

Figure 4 depicts the values of q for d ranging from -10^4 to 10^4 . The dark and green line represent the root of equation (17) and equation (D6), while the blue dots correspond to the results obtained through the SimCIM. Given that our simulations were conducted with $N = 1000$, the precision of the q ratio is limited to three decimal places. Consequently, the blue error bars are set to $\frac{1}{1000}$, reflecting the precision of $\frac{1}{N}$ for any given N . It is observed that $q(d)$ starts at $d = -1$ and then rapidly grows and stays near $\frac{1}{2}$ for $d \in [-0.1, 0.1]$, then follows a power law for $d \in [1, 10]$, and then saturates and tends to 1. We fitted a line for $d \in [1, 10]$ (on a log-log scale), and it follows $q(d) = 0.61 \cdot d^{0.13}$. As the interaction matrix is ordered and follows a hierarchical pattern, this likely underlies the observed power law trend for d values greater than 1 and less than 10. At $d = 10$, where the saturation begins and the power law behavior ends, the value of q is approximately 0.81.

B. D-wave Benchmarking and Fidelity Analysis

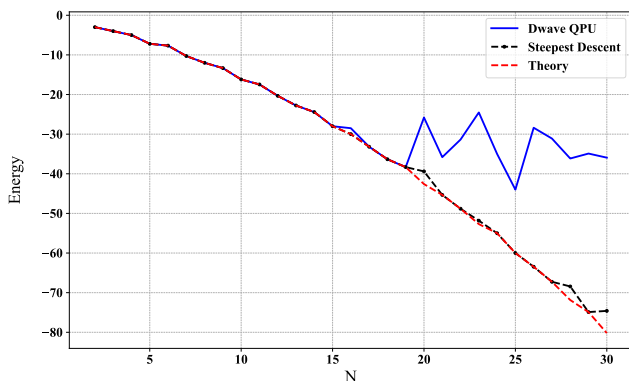


FIG. 5. Benchmarking results of the D-Wave quantum annealer and the steepest descent algorithm for problem sizes in the range $[2, 30]$ with $d = 1$. The energy values are compared against theoretical predictions. The D-Wave QPU shows significant deviation from theoretical values starting at $N = 20$. While the problem is polynomial, the D-Wave QPU cannot reach the ground state, making it a useful benchmark for assessing the fidelity of the QPU. The steepest descent algorithm generally reaches the ground state but sometimes gets trapped in local minima very close to the true ground state.

The performance of Ising solvers, such as the D-Wave quantum annealer, depends not only on their ability to optimize complex energy landscapes but also on how accurately the Ising Hamiltonian is encoded into the physical hardware. Errors in encoding, noise, or hardware imperfections can significantly degrade solution quality. To assess this aspect independently, we employed our benchmark interaction matrix $J^{(N,d)}$, which has an analytical ground state. As we demonstrated, finding the ground state of this matrix is a problem in P (Polynomial time), making it an ideal tool to evaluate the fidelity of encoding while isolating it from the solver’s optimization capabilities.

By leveraging $J^{(N,d)}$, we were able to directly compare the results from the D-Wave system with exact theoretical solutions. This enabled us to assess how accurately the D-Wave maps the mathematical problem onto its hardware, providing insights into potential limitations stemming from encoding errors. This method allows for a clearer distinction between encoding fidelity and the solver’s capacity to minimize energy.

Figure 5 presents the benchmarking results for the D-Wave system alongside the Steepest Descent (SD) algorithm, across problem sizes ranging from $N = 2$ to $N = 30$, with $d = 1$. For smaller problem sizes ($N \leq 20$), the D-Wave results align closely with both SD and the exact theoretical solutions. However, for larger problem sizes ($N > 20$), deviations become apparent, highlighting the challenges of encoding accuracy as the complexity of the fully connected

problem increases.

In contrast, as discussed in Section (V), the Simulated Coherent Ising Machine (SimCIM) demonstrated the capability to consistently reach the ground state for problem sizes as large as $N = 1000$. As a simulated algorithm, SimCIM operates without the hardware-based encoding limitations inherent in physical systems like D-Wave. This emphasizes the crucial role of encoding fidelity in benchmarking physical quantum annealers, as SimCIM’s performance was unaffected by such constraints.

The SD algorithm, often used as a post-processing tool for D-Wave results, was also evaluated as a standalone solver. Its solutions closely track the theoretical ground states across all problem sizes, indicating that the deviations observed in D-Wave results stem primarily from encoding fidelity rather than optimization performance.

VI. CONCLUSION

In this study, we introduced a novel class of fully connected Ising model. To analytically solve this class, we reformulated the discrete Ising Hamiltonian into a continuous framework, enabling us to determine the exact ground state. This reformulation represents a significant advancement in the analytical treatment of complex Ising systems.

Our analytical solutions were validated through numerical experiments with brute-force calculations, the Simulated Coherent Ising Machine (SimCIM), and the D-Wave quantum computer. The results demonstrated perfect agreement between brute-force calculations and our method for small-scale systems, as well as between SimCIM and our approach for larger systems. However, significant deviations were observed in the D-Wave quantum solver’s results, as shown in Figure 5. These deviations were initially examined for small-scale problems, and the analysis was extended to larger problem sizes, where the deviations persisted and became more pronounced, highlighting limitations in current quantum hardware for this class of problems.

The continuous formulation of the Ising Hamiltonian expands the potential for analytically solving diverse Ising problems, paving the way for future advancements in quantum simulation and computation. Furthermore, this new class of Ising models offer a robust testbed for assessing the fidelity of Ising minimizers, eliminating the need for computationally expensive brute-force validation.

ACKNOWLEDGMENT

We would like to express our gratitude to Dr. Behrouz Askari and Dr. G. Reza Jafari for their valuable comments and fruitful discussions. Their input, though brief, was appreciated and added value to the progression of this work.

- [1] S. G. Brush, *Reviews of modern physics* **39**, 883 (1967).
- [2] F. Barahona, *Journal of Physics A: Mathematical and General* **15**, 3241 (1982).
- [3] Y. Haribara, S. Utsunomiya, and Y. Yamamoto, *Entropy* **18**, 151 (2016).
- [4] D. E. Knuth, *SIGACT News* **6**, 15–16 (1974).
- [5] B. Cipra, *SIAM News* **33**, 1 (2000).
- [6] R. M. Karp, *Reducibility among combinatorial problems* (Springer, 2010).
- [7] V. Černý, *Journal of optimization theory and applications* **45**, 41 (1985).
- [8] H. M. Salkin and C. A. De Kluyver, *Naval Research Logistics Quarterly* **22**, 127 (1975).
- [9] T. R. Jensen and B. Toft, *Graph coloring problems* (John Wiley & Sons, 2011).
- [10] J. Gramm, J. Guo, F. Hüffner, and R. Niedermeier, *Journal of Experimental Algorithmics (JEA)* **13**, 2 (2009).
- [11] A. D. King, J. Raymond, T. Lanting, R. Harris, A. Zucca, F. Altomare, A. J. Berkley, K. Boothby, S. Ejtemaee, C. Enderud, *et al.*, *Nature* **617**, 61 (2023).
- [12] M. W. Johnson, M. H. Amin, S. Gildert, T. Lanting, F. Hamze, N. Dickson, R. Harris, A. J. Berkley, J. Johansson, P. Bunyk, *et al.*, *Nature* **473**, 194 (2011).
- [13] A. D. King, A. Nocera, M. M. Rams, J. Dziarmaga, R. Wiersema, W. Bernoudy, J. Raymond, N. Kaushal, N. Heinsdorf, R. Harris, *et al.*, arXiv preprint arXiv:2403.00910 (2024).
- [14] A. Marandi, Z. Wang, K. Takata, R. L. Byer, and Y. Yamamoto, *Nature Photonics* **8**, 937 (2014).
- [15] T. Inagaki, K. Inaba, R. Hamerly, K. Inoue, Y. Yamamoto, and H. Takesue, *Nature Photonics* **10**, 415 (2016).
- [16] P. L. McMahon, A. Marandi, Y. Haribara, R. Hamerly, C. Langrock, S. Tamate, T. Inagaki, H. Takesue, S. Utsunomiya, K. Aihara, *et al.*, *Science* **354**, 614 (2016).
- [17] T. Inagaki, Y. Haribara, K. Igarashi, T. Sonobe, S. Tamate, T. Honjo, A. Marandi, P. L. McMahon, T. Umeki, K. Enbutsu, *et al.*, *Science* **354**, 603 (2016).
- [18] H. Goto, *Scientific reports* **6**, 21686 (2016).
- [19] H. Goto, K. Tatsumura, and A. R. Dixon, *Science advances* **5**, eaav2372 (2019).
- [20] H. Goto, K. Endo, M. Suzuki, Y. Sakai, T. Kanao, Y. Hamakawa, R. Hidaka, M. Yamasaki, and K. Tatsumura, *Science Advances* **7**, eabe7953 (2021).
- [21] S. Kirkpatrick, C. D. Gelatt, and M. P. Vecchi, *Science* **220**, 671 (1983).
- [22] P. J. Van Laarhoven, E. H. Aarts, P. J. van Laarhoven, and E. H. Aarts, *Simulated annealing* (Springer, 1987).
- [23] D. Bertsimas and J. Tsitsiklis, *Statistical science* **8**, 10 (1993).
- [24] W. Huang, D. A. Kitcheav, S. T. Dacek, Z. Rong, A. Urban, S. Cao, C. Luo, and G. Ceder, *Physical Review B* **94**, 134424 (2016).
- [25] Y. I. Dublennykh, *Physical Review Letters* **109**, 167202 (2012).
- [26] P. Bak and R. Bruinsma, *Physical Review Letters* **49**, 249 (1982).
- [27] U. Löw, V. Emery, K. Fabricius, and S. Kivelson, *Physical Review Letters* **72**, 1918 (1994).
- [28] M. Ercsey-Ravasz and Z. Toroczkai, *Nature Physics* **7**, 966 (2011).
- [29] Y. Yamamoto, K. Aihara, T. Leleu, K.-i. Kawarabayashi, S. Kako, M. Fejer, K. Inoue, and H. Takesue, *npj Quantum Information* **3**, 49 (2017).
- [30] F. Chen, B. Isakov, T. King, T. Leleu, P. McMahon, and T. Onodera, *cim-optimizer: a simulator of the Coherent Ising Machine* (2022).
- [31] Q.-G. Zeng, X.-P. Cui, B. Liu, Y. Wang, P. Mosharev, and M.-H. Yung, *Communications Physics* **7**, 249 (2024).
- [32] D. E. Knuth, *Mathematics of Computation* **61**, 277 (1993).

Appendix A: CIM Hyperparameters

The hyperparameters for SimCIM were tuned with Bayesian optimization. The hyperspace for finding the ground state is shown in Table I. In this table, the hyperparameters CAC- α and CAC- β were optimized within a range of $\pm 20\%$ of their initial values, while CAC- τ and CAC- γ were manually set and were not subject to optimization. The time span was fixed at 10000 to ensure we reach the most optimal solution. This approach allowed us to reach the ground state for different values of d .

Hyperparameter	Value	Search Space
CAC- α	0.7	[0.56, 0.84] ($\pm 20\%$)
CAC- β	0.25	[0.2, 0.3] ($\pm 20\%$)
CAC- τ	150	Manually set
CAC- γ	0.01	Manually set

TABLE I. Hyperspace of the Simulated Coherent Ising Machine with Bayesian Optimization

Appendix B: Evaluating Integral

By expanding Equation (23), we can obtain

$$H_{\Lambda}(d, \mathbf{q}) = \int_0^1 \int_0^1 \frac{N^2}{2} x^d \prod_{\alpha=1}^{\Lambda} \text{sgn}(x - q_{\alpha}) \text{sgn}(y - q_{\alpha}) dx dy + \int_0^1 \int_0^1 \frac{N^2}{2} y^d \prod_{\alpha=1}^{\Lambda} \text{sgn}(x - q_{\alpha}) \text{sgn}(y - q_{\alpha}) dx dy \quad (\text{B1})$$

Both parts are the same integral, except that the symbols x and y are swapped. We can therefore rewrite Equation (B1) as:

$$H_{\Lambda}(d, \mathbf{q}) = N^2 \int_0^1 \int_0^1 x^d \prod_{\alpha=1}^{\Lambda} \text{sgn}(x - q_{\alpha}) \text{sgn}(y - q_{\alpha}) dx dy \quad (\text{B2})$$

Using Fubini's Theorem, we obtain:

$$H_{\Lambda}(d, \mathbf{q}) = N^2 \int_0^1 x^d \prod_{\alpha=1}^{\Lambda} \text{sgn}(x - q_{\alpha}) dx \int_0^1 \text{sgn}(y - q_{\alpha}) dy \quad (\text{B3})$$

Now we can omit the sign functions and by considering q_0 and $q_{\Lambda+1}$, we have:

$$H_{\Lambda}(d, \mathbf{q}) = N^2 \left(\sum_{\alpha=0}^{\Lambda} \int_{q_{\alpha}}^{q_{\alpha+1}} x^d (-1)^{\Lambda-\alpha} dx \right) \left(\sum_{\alpha=0}^{\Lambda} \int_{q_{\alpha}}^{q_{\alpha+1}} (-1)^{\Lambda-\alpha} dy \right) \quad (\text{B4})$$

where this integral could be solved as bellow:

$$H_\Lambda(d, \mathbf{q}) = N^2 \left(\sum_{\alpha=0}^{\Lambda} \left[\frac{x^{d+1}}{d+1} (-1)^{\Lambda-i} \right]_{q_\alpha}^{q_{\alpha+1}} \right) \left(\sum_{\alpha=0}^k [y(-1)^{\Lambda-\alpha}]_{q_\alpha}^{q_{\alpha+1}} \right) \quad (\text{B5})$$

which leads to Equation (24) \square .

Appendix C: Uniqueness of Ground State Pattern

By taking the derivative of H_1 and equating it to 0 we obtain:

$$2q_1^{d+1} - 1 = -(d+1)q_1^d(2q_1 - 1) \quad (\text{C1})$$

Using Equation (C1) and Equation (24), we can write:

$$H_1(d, q_1) = -(2q_1 - 1)^2 q_1^d \quad (\text{C2})$$

which is always a negative number. For $d > 0$, it can be shown that for each i , we have $q_i > \frac{1}{2}$. From Equation (C1), we can write:

$$2q_1^{d+1} + (d+1)q_1^d(2q_1 - 1) = 1 \quad (\text{C3})$$

By reordering the left hand side of Equation (C3) :

$$q_1^d(2q_1 + (d+1)(2q_1 - 1)) = 1 \quad (\text{C4})$$

The expression in parenthesis on the left hand side of Equation (C4) is strictly greater than 1 for $d > 0$:

$$2q_1 + (d+1)(2q_1 - 1) > 1 \quad (\text{C5})$$

which can be simplified further:

$$(2q_1 - 1)(d+2) > 0 \quad (\text{C6})$$

from which we can readily verify that $q_1 > \frac{1}{2}$ for $d > 0$. Using this result, it can be shown that $H_1(d, q_1)$ is convex on the interval $q_1 > \frac{1}{2}$ and $d > 0$, by taking its second derivative:

$$\frac{\partial^2 H_1}{\partial q_1^2} = 2q_1^{d-1}(4q_1 + d(2q_1 - 1)), \quad (\text{C7})$$

and observing that for $q_1 > \frac{1}{2}$ and $d > 0$, Equation (C7) is strictly positive. The convexity of $H_1(d, q_1)$ on interval $q_1 > \frac{1}{2}$ and $d > 0$, implies the uniqueness of q_1 . This can be shown by observing that $\frac{\partial H_1}{\partial q_1}|_{q_1=\frac{1}{2}} < 0$ and $\frac{\partial H_1}{\partial q_1}|_{q_1=1} > 0$. Thus, the mean value theorem implies that there exists a zero for the first derivative of $H_1(d, q_1)$ with respect to q_1 , on interval $[\frac{1}{2}, 1]$ and by convexity of $H_1(d, q_1)$ on the interval, we can conclude that the root is unique.

Appendix D: Finding Ground State Pattern

For $\Lambda \geq 2$, first we find the critical points of Equation (24). Taking the derivative, with respect to q_j results in Equation

(D1):

$$\frac{\partial H_\Lambda}{\partial q_j} = (-1)^{j+1} 2q_j^d \left((-1)^\Lambda + 2 \sum_{i=1}^{\Lambda} (-1)^{i+1} q_i \right) + (-1)^{j+1} \frac{2}{1+d} \left((-1)^\Lambda + 2 \sum_{i=1}^{\Lambda} (-1)^{i+1} q_i^{d+1} \right) \quad (\text{D1})$$

At a critical point all of the derivatives, as shown in Equation (D1), must be zero. Consequently, for $\Lambda \geq 2$ and $j \in [1, \Lambda - 1]$, sum of the derivatives of Equation (24) with respect to q_j and q_{j+1} must also be 0. Thus, we can write:

$$\frac{\partial H_\Lambda}{\partial q_j} + \frac{\partial H_\Lambda}{\partial q_{j+1}} = 2(-1)^j (q_j^d - q_{j+1}^d) \times \left[(-1)^\Lambda + 2 \sum_{n=1}^{\Lambda} (-1)^{n+1} q_n \right] = 0 \quad (\text{D2})$$

For Equation (D2) to hold, we must have:

$$(-1)^\Lambda + 2 \sum_{n=1}^{\Lambda} (-1)^{n+1} q_n = 0 \quad (\text{D3})$$

Equation (D3) implies that, the Hamiltonian in Equation (24) in critical points for $\Lambda \geq 2$, is 0. The only remaining interesting points are the boundaries of the domain of the Hamiltonian. The first two boundaries is to set $q_1 = 0$ and $q_\Lambda = 1$. First we show that if we have $q_\Lambda \rightarrow 1$, then $H_\Lambda(q_\Lambda \rightarrow 1) \rightarrow H_{\Lambda-1}$:

$$H_\Lambda(d, q_\Lambda \rightarrow 1) = \frac{N^2}{1+d} \left((-1)^\Lambda + 2(-1)^{\Lambda+1} + 2 \sum_{i=1}^{\Lambda-1} (-1)^{i+1} q_i \right) \left((-1)^\Lambda + 2(-1)^{\Lambda+1} + 2 \sum_{i=1}^{\Lambda-1} (-1)^{i+1} q_i^{d+1} \right) \quad (\text{D4})$$

and this can be simplified as:

$$H_\Lambda(d, q_\Lambda \rightarrow 1) = \frac{N^2}{1+d} \left((-1)^{\Lambda-1} + 2 \sum_{i=1}^{\Lambda-1} (-1)^{i+1} q_i \right) \times \left((-1)^{\Lambda-1} + 2 \sum_{i=1}^{\Lambda-1} (-1)^{i+1} q_i^{d+1} \right) \quad (\text{D5})$$

which is equal to $H_{\Lambda-1}(d, \mathbf{q})$. Since the same argument for the critical points of H_Λ can also be made for $H_{\Lambda-1}$, we can conclude that the global minimum of $H_{\Lambda-1}$ must also lie on its boundary and the same argument can be made for $H_{\Lambda-2}$ by letting $q_{\Lambda-1} \rightarrow 1$ and obtaining $H_{\Lambda-2}$. We may continue in this manner, until we reach H_1 , which its minimum value is given in Equation (17). The same procedure can be shown when $q_1 \rightarrow 0$, in which case, we also have $H_\Lambda \rightarrow H_{\Lambda-1}$, with the difference that the indices for q_i s shift by one, i.e. in the new Hamiltonian, $q_{i+1} \rightarrow q_i$.

For $d \leq -1$, Equation (23) doesn't converge, as it has a singularity at $x = y = 0$. To overcome this issue, we can simply keep the lower limit of integral in Eq. (23) as $\frac{1}{N}$ and avoid the

singularity. Without any loss of generality, and by a similar approach as before, we can find the extended expression for $q(d)$:

$$\left(1 + \left(\frac{1}{N}\right)^{d+1} - 2q^{d+1}\right) + (d+1)\left(1 + \frac{1}{N} - 2q\right)q^d = 0. \quad (\text{D6})$$

The proof for this case follows a similar line of reasoning as the proof for $d > -1$, with appropriate adjustments for the modified lower limit of the integral. While this extended form is more general, we chose to present the proof for $d > -1$ in detail as it is more concise and illustrates the key principles without the additional complexity introduced by the regularization term.

Appendix E: Permutation Invariance of $J^{(N,d)}$

Here, we examine another property of this class of interaction matrices. This characteristic allows us to determine the interaction matrix for any given spin configuration, assuming that the spin configuration represents the ground state of the interaction matrix. This is achieved by exploiting the properties of $J^{N,d}$. Rewriting equation (5) in vector-

matrix notation (and discarding the factor of $\frac{1}{2}$), we have:

$$H = \mathbf{s}^T J \mathbf{s} \quad (\text{E1})$$

Now note that H is invariant under the following transformation:

$$H = \mathbf{s}^T P^T P J P^T P \mathbf{s} = \mathbf{s}'^T J' \mathbf{s}', \quad (\text{E2})$$

where P is a permutation matrix. As we have shown, the ratio q can be any value between $[0, 1]$. Considering this, the \mathbb{Z}_2 symmetry and the permutation invariance of J , any configuration of \mathbf{s} can be represented as the ground state of $J^{N,d}$. To further illustrate this, note that any configuration \mathbf{s} , has fixed number of up and down spins, and the ratio of spins to the system size (q) is always between 0 and 1. Assume that the said configuration has two clusters of up and down spins, and is not scrambled. Now to find the proper interaction matrix for the ratio q , we can simply select d in accordance with Equation (D6) and Figure 4. Now, to unscramble the configuration, we can use permutation matrices repeatedly. This allows us to sort this configuration to two clusters of up and down spins (using Equation (E2)) and with that, we can also sort the interaction matrix.